Air Pollution
ENV-409

Topics in numerical modeling

Computational modeling

A conceptual and quantitative mathematical model of the atmosphere can allow us to

- link source emissions, atmospheric composition, and impacts
- test hypotheses regarding magnitude of contributing processes to observations
- evaluate emission control strategies
- predict future air quality and climate scenarios based on projected changes in emissions (adaptation)

$$\frac{\Delta(c_1, c_2, \ldots, c_n)}{\Delta(E_1, E_2, \ldots, E_n)}$$

Some categorization of models:

- statistical/mechanistic
- stochastic/deterministic

We will discuss mechanistic, deterministic models.

"All models are wrong, but some are useful."
- George P. Box

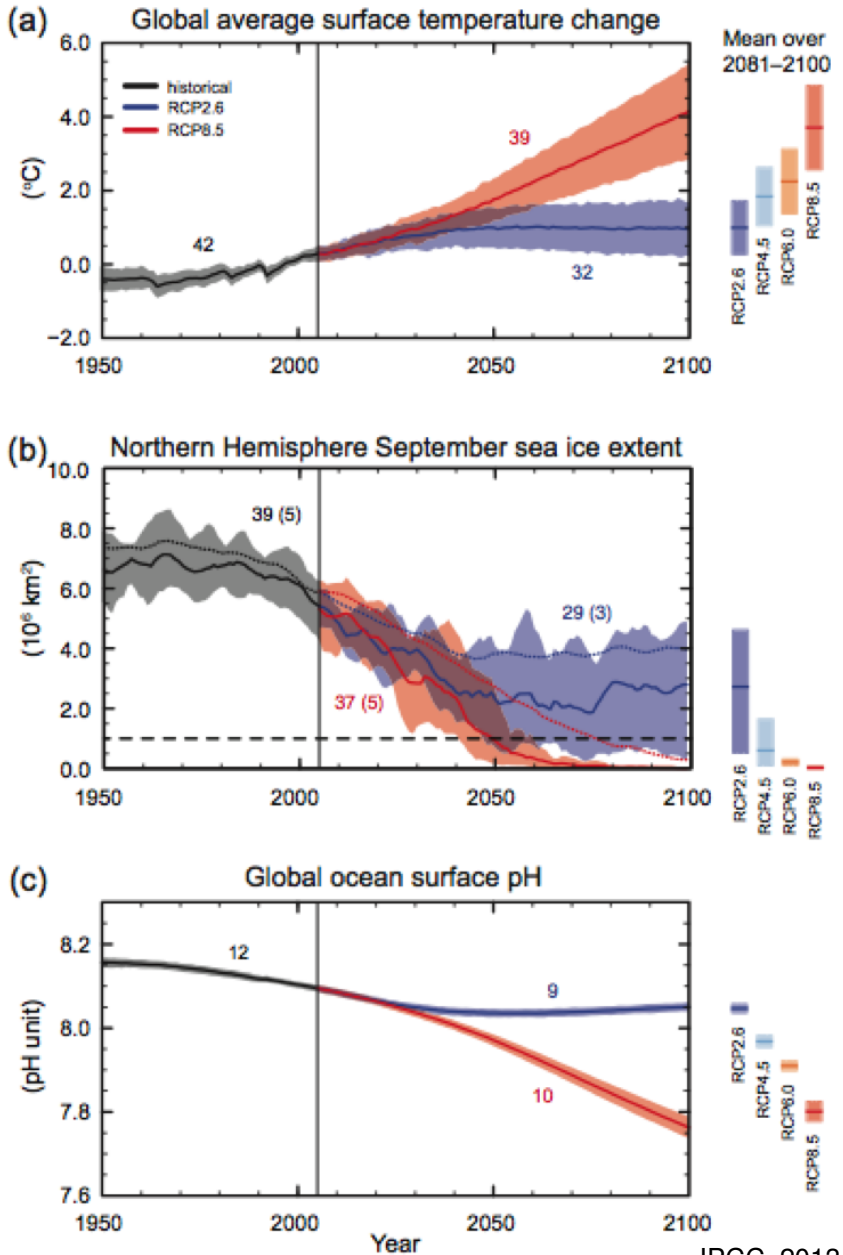

IPCC, 2013

Example applications

The Costs, Air Quality, and Human Health Effects of Meeting Peak Electricity Demand with Installed Backup Generators

ELISABETH A. GILMORE,*
LESTER B. LAVE, AND PETER J. ADAMS
Engineering and Public Policy, Chemical Engineering, Civil Engineering and Tepper Business School, Carnegie Mellon University, Pittsburgh, Pennsylvania 15213

VOL. 40, NO. 22, 2006 / ENVIRONMENTAL SCIENCE & TECHNOLOGY

Peak ozone

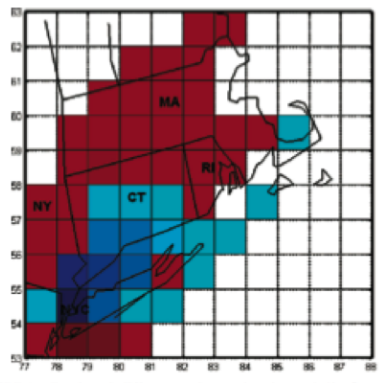

Daily average PM

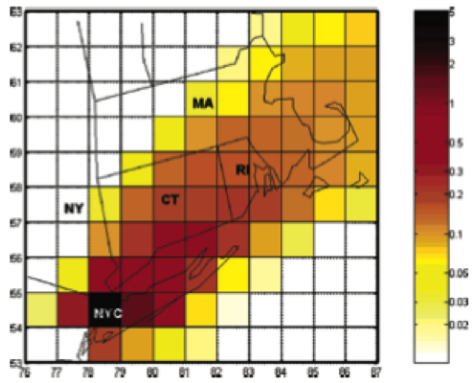

Effects of Ethanol (E85) versus Gasoline Vehicles on Cancer and Mortality in the United States

MARK Z. JACOBSON*
Department of Civil and Environmental Engineering, Stanford University, Stanford, California 94305-4020

Environ. Sci. Technol. **2007**, *41*, 4150−4157

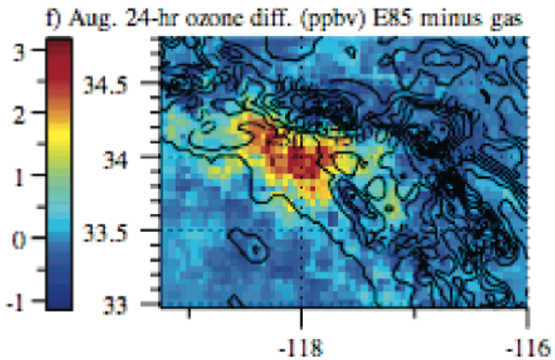

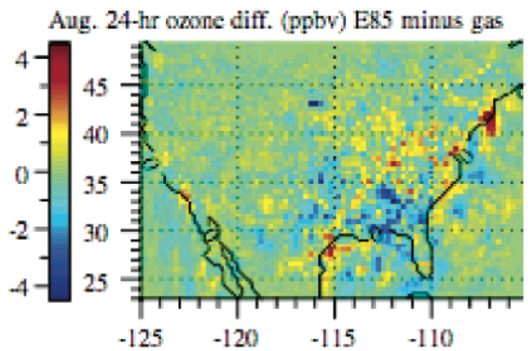

Time and spatial scales

Spatial scales

- micro (∼1 km)
- meso (∼50 km)
- synoptic (∼300 km)
- global

- molecular
- turbulent eddies
- plume
- cloud
- urban airshed
- regional
- global

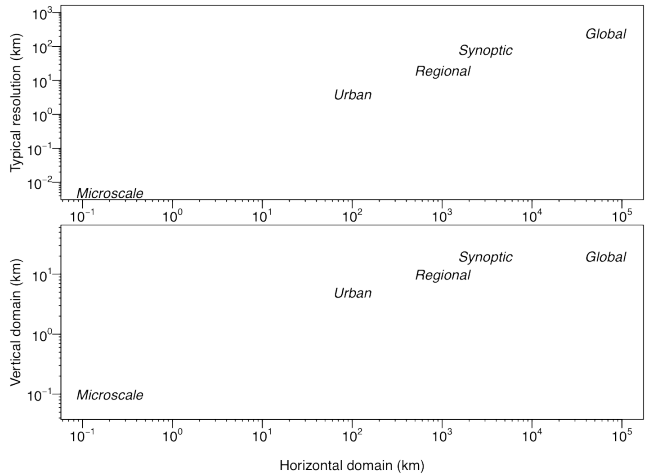

adapted from Seinfeld and Pandis, 2006

Time scales (by process)

- electron transfer
- molecular vibrations
- emission
- reaction
- condensation/ evaporation (phase-partitioning)

- deposition
- diffusion
- advection
- convection

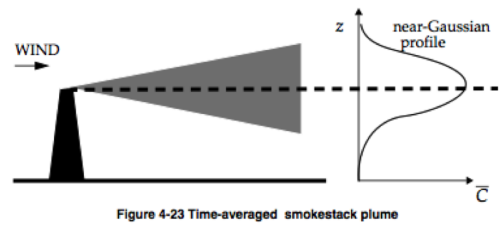

Figure 4-23 Time-averaged smokestack plume

Jacob, 1999

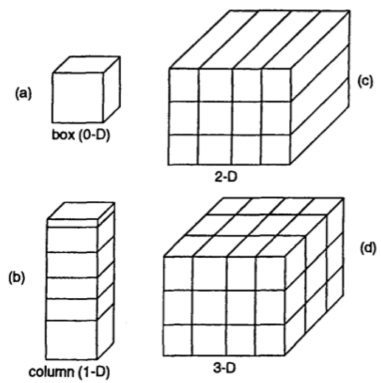

FIGURE 25.3 Schematic depiction of (a) a box model (zero-dimensional), (b) a column model (one-dimensional), (c) a two-dimensional model, and (d) a three-dimensional model.

Seinfeld and Pandis, 2006

Model formulation

Frame of reference

- fixed (Eulerian)
- moving (Lagrangian)

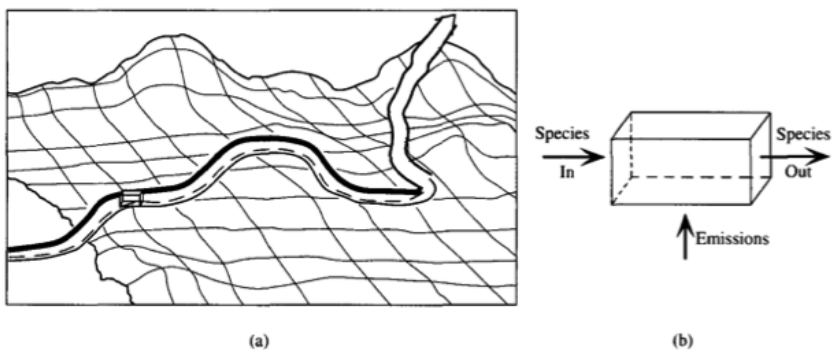

FIGURE 25.2 Schematic depiction of (a) a Lagrangian model and (b) a Eulerian model.

Seinfeld and Pandis, 2006

Chemistry-meteorology

- assimilated meteorology
- coupled climate-chemistry/ meteorology-chemistry

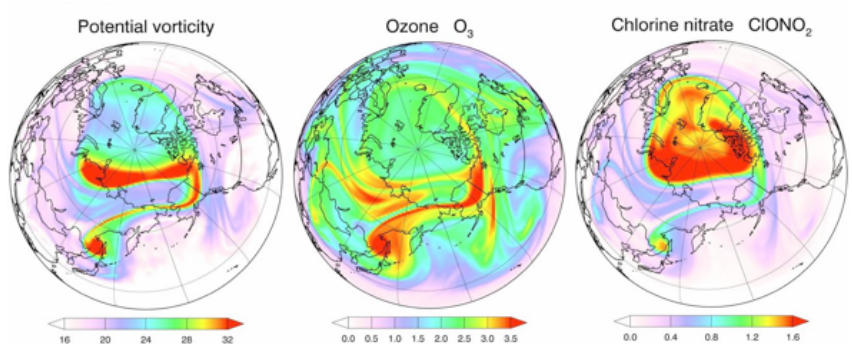

source: NCAR

General circulation models (GCMs)

- Large-scale motions of fluid
- Radiative transfer

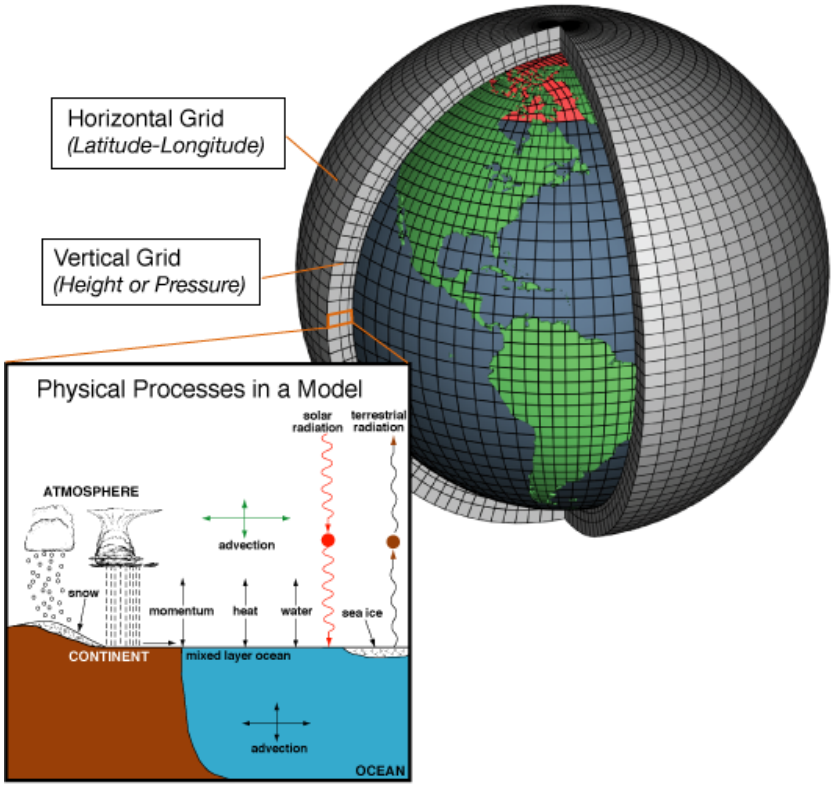

source: NOAA

Chemical transport models (CTMs)

Detailed continuity equations for chemical species

$$\frac{\partial c_i}{\partial t} + \nabla \cdot (\mathbf{u} c_i) = R_i(c_1, c_2, \ldots, c_n) + E_i - S_i$$

Goddard Institute for Space Studies Models I and II:

TABLE I. Fundamental equations.

Conservation of momentum: (Newton's second law of motion)	$\frac{d\mathbf{V}}{dt} = -2\boldsymbol{\Omega} \times \mathbf{V} - \rho^{-1}\nabla p + \mathbf{g} + \mathbf{F}$	(T1)
Conservation of mass: (continuity equation)	$\frac{d\rho}{dt} = -\rho\nabla \cdot \mathbf{V} + C - D$	(T2)
Conservation of energy: (first law of thermodynamics)	$\frac{dI}{dt} = -p\frac{d\rho^{-1}}{dt} + Q$	(T3)
Ideal gas law: (approximate equation of state)	$p = \rho RT$	(T4)

Notation

$\mathbf{V}$	velocity relative to rotating earth
t	time
$\frac{d}{dt}$	total time derivative $\left[= \frac{\partial}{\partial t} + \mathbf{V} \cdot \nabla\right]$
$\boldsymbol{\Omega}$	planet's angular rotation vector
ρ	atmospheric density
$\mathbf{g}$	apparent gravity [=true gravity $- \boldsymbol{\Omega} \times (\boldsymbol{\Omega} \times \mathbf{r})$]
$\mathbf{r}$	position relative to planet's center
$\mathbf{F}$	force per unit mass
C	rate of creation of (gaseous) atmosphere
D	rate of destruction of atmosphere
I	internal energy per unit mass [$=c_v T$]
Q	heating rate per unit mass
R	gas content
c_v	specific heat at constant volume.

Hansen et al., 1983

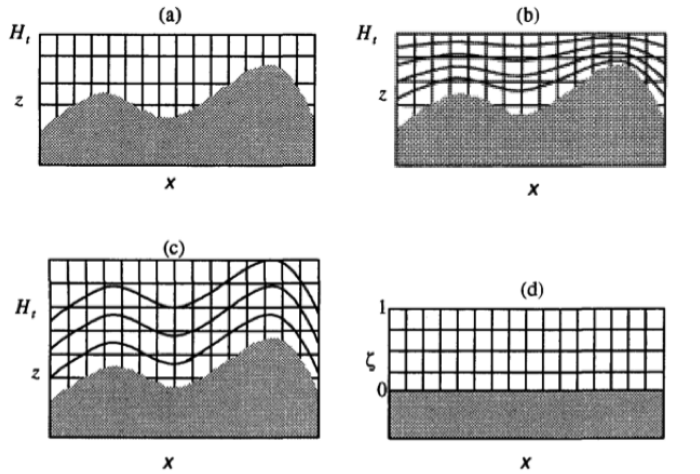

FIGURE 25.6 Coordinate transformation for uneven terrain: (a) two-dimensional terrain in $x - z$ space; (b) same as (a) but with contours of constant ζ superimposed; (c) same as (a) but with contours of constant z' superimposed; (d) two-dimensional terrain in $x - \zeta$ computational space (the terrain is indicated by the shaded region).

Seinfeld and Pandis, 2006

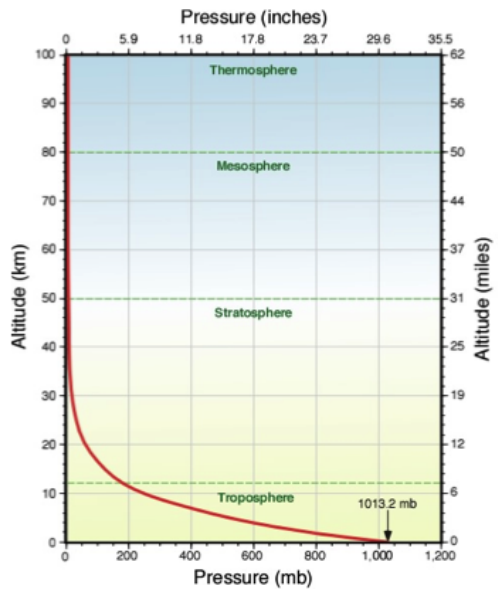

http://www.physicalgeography.net

Terrain effects and boundary layer height

Given z = absolute height, h = terrain height, H_m = mixing height, we can define a new vertical coordinate:

$$z' = z - h(x, y)$$

Or a terrain-following coordinate transformation:

$$\zeta = \frac{z - h(x, y)}{H_m(x, y, t) - h(x, y)}$$

Pressure-based coordinate system

Given p = pressure at a given height z, p_s = surface pressure, p_t = pressure at top of modeling domain (e.g., 0.1 atm for the troposphere)

$$\sigma(p) = \frac{p - p_t}{p_s - p_t}$$

Nesting, adaptive gridding

We can resolve atmospheric processes at various scales with creating meshing as long as emissions and other required information (e.g., meteorological variables) are available at the same resolution. Coarser models can provide boundary values or initial conditions for the more finely resolved model, etc.

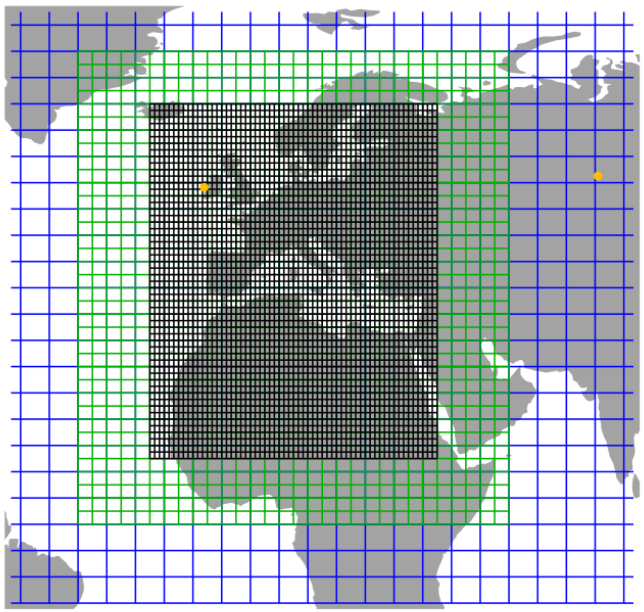

Fig. 1. Horizontal resolution of the TM5 version that zooms in over Europe. Globally (blue), the resolution is 6°×4° (longitude×latitude). Over Europe, the resolution is refined in two steps via 3°×2° (green) to 1°×1° (black). The two yellow dots denote the geographical locations of the Mace Head (Ireland) and Omsk (Russia) sampling stations (see Sect. 3.2).

Krol et al., 2005

Figure 3. Adapted grid during a biomass burning plume simulation with AG-CMAQ.

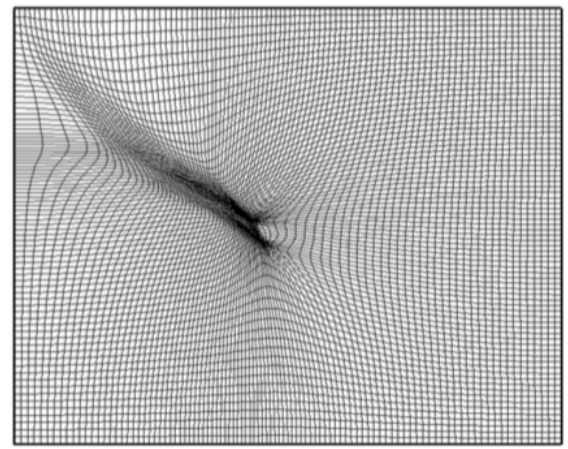

Garcia-Menendez and Odman, 2011

Processes

The concentration of species i is a function of space and time: $c_i = c_i(\mathbf{r}, t)$.

$$\frac{\partial c_i}{\partial t} = \left[\frac{\partial c_i}{\partial t}\right]_{\text{advection}} + \left[\frac{\partial c_i}{\partial t}\right]_{\text{dispersion}} + \left[\frac{\partial c_i}{\partial t}\right]_{\text{gas-phase chemistry}} + \left[\frac{\partial c_i}{\partial t}\right]_{\text{emission}} + \left[\frac{\partial c_i}{\partial t}\right]_{\text{wet/dry deposition}} + \left[\frac{\partial c_i}{\partial t}\right]_{\text{aerosol}} + \left[\frac{\partial c_i}{\partial t}\right]_{\text{aqueous-phase chemistry}}$$

Mass vs. number conservation for aerosols:

- mass is important for $PM_{2.5}$ and PM_{10} regulation, light scattering, and mass budget considerations.
- number is important for simulating new particle formation and aerosol-cloud interactions.

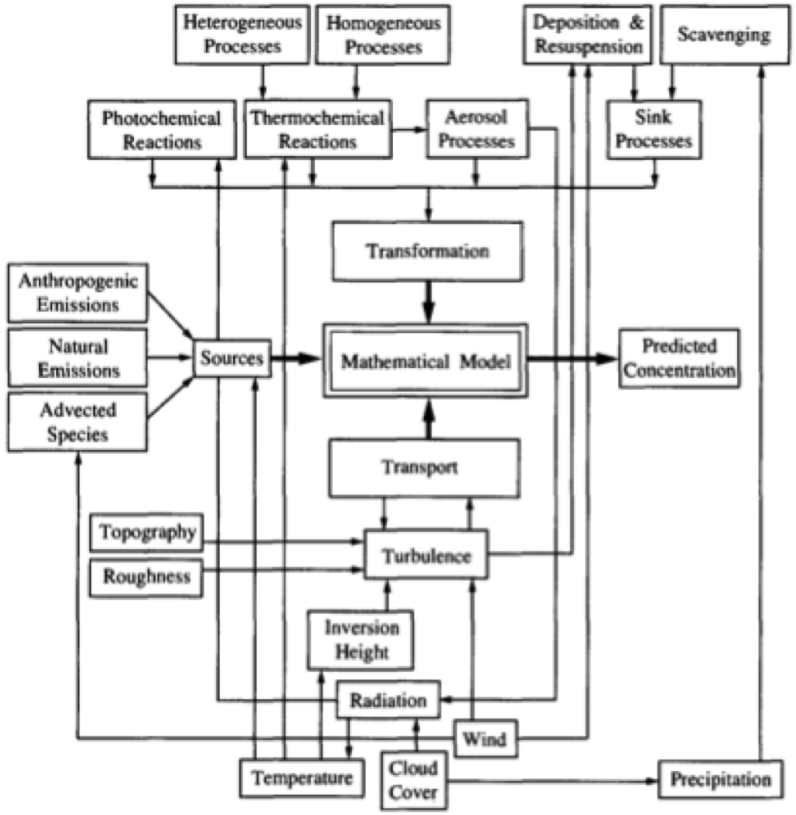

FIGURE 25.1 Elements of a mathematical atmospheric chemical transport model.

Operator splitting

Let $\mathbf{c}(t) = c(\mathbf{r}, t)$. We can define an operator $X = X(\Delta t)$ and its corresponding incremental operator ΔX:

$$X\,\mathbf{c}(t) = [\mathbf{c}(t + \Delta t)]_X \qquad = \mathbf{c}(t) + \int_t^{t+\Delta t} \left[\frac{\partial \mathbf{c}}{\partial \tau}\right] d\tau$$

$$\Delta X\,\mathbf{c}(t) = [\mathbf{c}(t + \Delta t) - \mathbf{c}(t)]_X = \int_t^{t+\Delta t} \left[\frac{\partial \mathbf{c}}{\partial \tau}\right] d\tau$$

Let X represent various processes:

- A Advection
- D Diffusion
- C Cloud
- G Gas-phase chemistry
- P Aerosol
- S Source/sink

Operators can be applied in sequence or in parallel.

Sequential operation:

$$\mathbf{c}(t + \Delta t) = (S \circ P \circ G \circ C \circ D \circ A)\,\mathbf{c}(t)$$

where $\circ$ denotes operator composition: $f(g(x)) = (f \circ g)(x)$.

Parallel operation:

$$\mathbf{c}(t + \Delta t) = \mathbf{c}(t) + (\Delta S + \Delta P + \Delta G + \Delta C + \Delta D + \Delta A)\,\mathbf{c}(t)$$

Example: advection equation

Operator splitting is also used to decouple the processes in space. Reverting back to representation of concentration as $c = c(\mathbf{r}, t)$, consider the advection equation:

$$\frac{\partial c}{\partial t} + \mathbf{u} \cdot \nabla c = 0$$

In Cartesion coordinates,

$$\frac{\partial c}{\partial t} = -u\frac{\partial c}{\partial x} - v\frac{\partial c}{\partial y} - w\frac{\partial c}{\partial x}$$

Applying the operators in parallel,

$$c(t + \Delta t) = c(t) + \left(\Delta A_x + \Delta A_y + \Delta A_z\right) c(t)$$

we can solve three one-dimensional equations instead of one three-dimensional equation:

$$\left[\frac{\partial c}{\partial t}\right]_x = -u\frac{\partial c}{\partial x}, \quad \left[\frac{\partial c}{\partial t}\right]_y = -v\frac{\partial c}{\partial y}, \quad \text{and} \quad \left[\frac{\partial c}{\partial t}\right]_z = -w\frac{\partial c}{\partial z}$$

Discretization. Discretizing the domain and defining the concentrations over this new domain,

$$c^n_{i,j,k} = c(x_i, y_j, z_k, t_n)$$
$$c^{n+1}_{i,j,k} = c(x_i, y_j, z_k, t_n + \Delta t)$$

Representation by finite difference. We can approximate with the simplest of (backward) finite difference approximations as

$$\frac{c^{n+1}_{i,j,k} - c^n_{i,j,k}}{\Delta t} = -\frac{u^n_{i,j,k}c^n_{i,j,k} - u^n_{i-1,j,k}c^n_{i-1,j,k}}{\Delta x}$$
$$\frac{c^{n+1}_{i,j,k} - c^n_{i,j,k}}{\Delta t} = -\frac{v^n_{i,j,k}c^n_{i,j,k} - v^n_{i,j-1,k}c^n_{i,j-1,k}}{\Delta y}$$
$$\frac{c^{n+1}_{i,j,k} - c^n_{i,j,k}}{\Delta t} = -\frac{w^n_{i,j,k}c^n_{i,j,k} - w^n_{i,j,k-1}c^n_{i,j,k-1}}{\Delta z}$$

Integration (by Euler's method). We get the solution with respect to advection as

$$c^{n+1}_{i,j,k} = c^n_{i,j,k} + \frac{u^n_{i-1,j,k}c^n_{i-1,j,k} - u^n_{i,j,k}c^n_{i,j,k}}{\Delta x}\Delta t + \frac{v^n_{i,j-1,k}c^n_{i,j-1,k} - v^n_{i,j,k}c^n_{i,j,k}}{\Delta y}\Delta t + \frac{w^n_{i,j,k-1}c^n_{i,j,k-1} - w^n_{i,j,k}c^n_{i,j,k}}{\Delta z}\Delta t$$

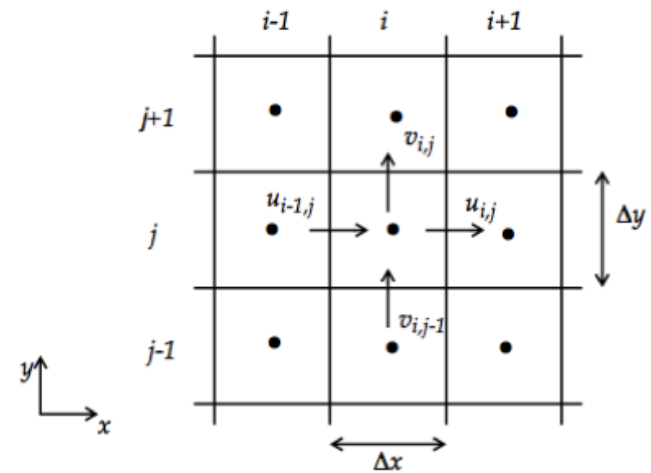

Figure 5-2 Spatial discretization of the continuity equation (only two dimensions are shown). Dots indicate gridpoints at which the concentrations are calculated, and lines indicate gridbox boundaries at which the transport fluxes are calculated.

Jacob, 1999

Example: Gas-phase chemical reaction and gas/particle partitioning

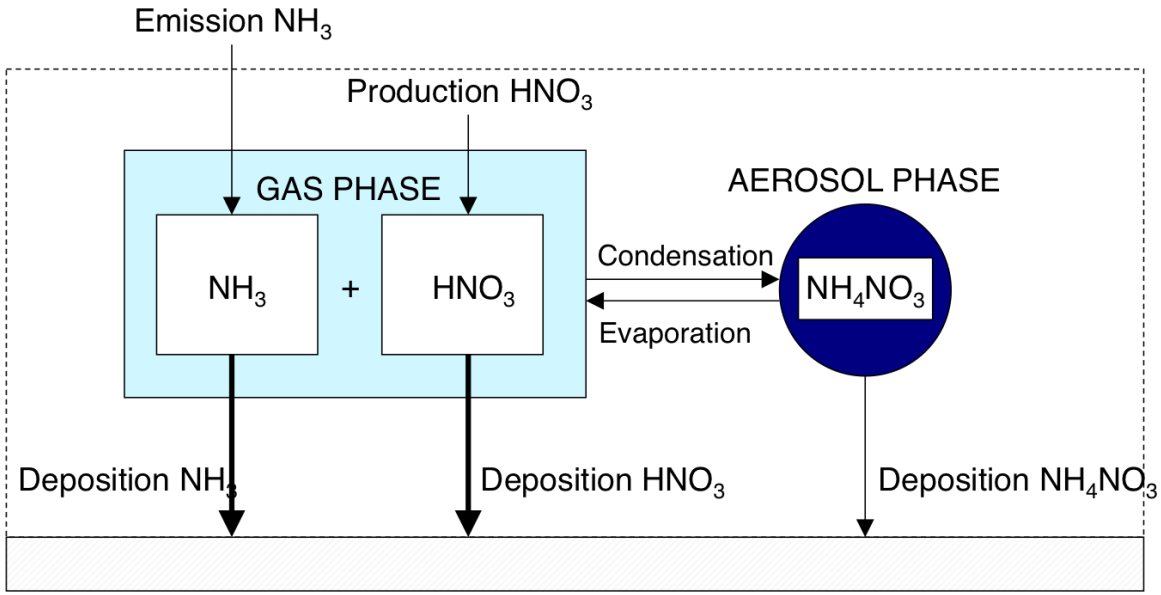

Adapted from Pandis and Seinfeld, 1990; Vayenas et al., 2005

Single box model including partitioning, deposition, emission, and reaction:

$$\frac{dc_{NH_3}}{dt} = \left(\frac{dc_{NH_3}}{dt}\right)_{\text{cond/evap}} - \frac{v_{NH_3}}{H} c_{NH_3} + E_{NH_3}$$

$$\frac{dc_{HNO_3}}{dt} = \left(\frac{dc_{HNO_3}}{dt}\right)_{\text{cond/evap}} - \frac{v_{HNO_3}}{H} c_{HNO_3} + R_{g,HNO_3}$$

$$\frac{dc_{NH_4NO_3}}{dt} = \left(\frac{dc_{NH_4NO_3}}{dt}\right)_{\text{cond/evap}} - \frac{v_{NH_4NO_3}}{H} c_{NH_4NO_3}$$

Sequential application of operator splitting:

$$c_{\mathrm{NH_3}}(t+\Delta t) = \left[S_{\mathrm{NH_3}}(\Delta t) \circ P_{\mathrm{NH_4NO_3}}(\Delta t) \circ E_{\mathrm{NH_3}}(\Delta t)\right] c_{\mathrm{NH_3}}(t)$$

$$c_{\mathrm{HNO_3}}(t+\Delta t) = \left[S_{\mathrm{HNO_3}}(\Delta t) \circ P_{\mathrm{NH_4NO_3}}(\Delta t) \circ R_{\mathrm{HNO_3}}(\Delta t)\right] c_{\mathrm{HNO_3}}(t)$$

$$c_{\mathrm{NH_4NO_3}}(t+\Delta t) = \left[S_{\mathrm{NH_4NO_3}}(\Delta t) \circ P_{\mathrm{NH_4NO_3}}(\Delta t)\right] c_{\mathrm{NH_4NO_3}}(t)$$

Illustration:

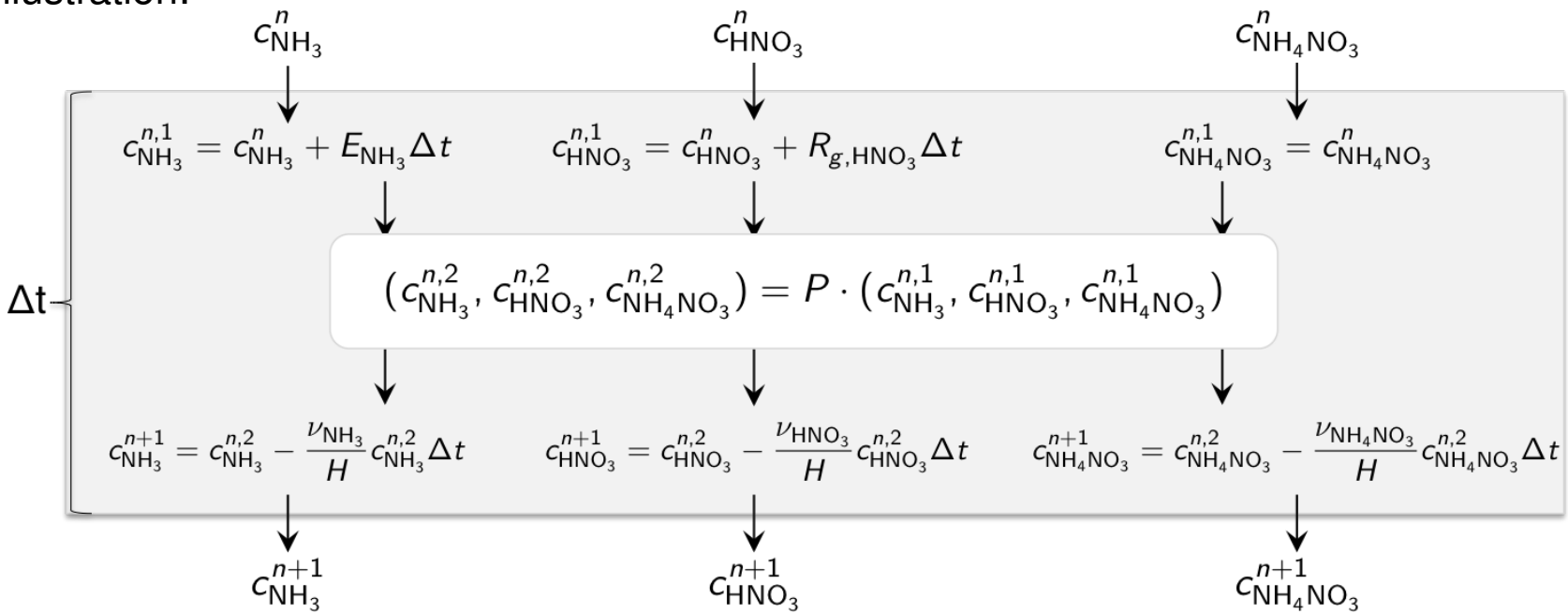

Modularity of operator splitting

Decoupled treatment of many processes permits many advantages.

- Programatically, we can replace the underlying mechanism or its implementation in this subroutine/module without affecting how the other processes are simulated.
- The most appropriate solver can be used for each module (i.e., for gas-phase kinetics, condensation/evaporation, etc.).
- However, concentrations must not change too rapidly at each time step to minimize approximation error.

Linear vs. nonlinear operations

Let us consider whether a function is linear or nonlinear.
Properties of linear functions:

$$f(x+y) = f(x) + f(y)$$
$$f(ax) = af(x)$$

Function applied to average of inputs corresponds to average of outputs:

$$\frac{1}{n}\sum_{i=1}^{n} f(x_i) = f\left(\frac{1}{n}\sum_{i=1}^{n} x_i\right) \quad \text{or, more concisely,} \quad \langle f(\mathbf{x})\rangle = f(\langle \mathbf{x}\rangle)$$

Example. Does $2f(x) = f(2x)$?

Linear function:

$$f(x) = x$$
$$2f(x) = 2x = f(2x)$$

Non-linear function:

$$f(x) = x^2$$
$$2f(x) \neq 4x^2 = f(2x)$$

Examples of linear and nonlinear operations

Gaussian plume model (solution to continuous release)

$$c(x,y,z) = \frac{q}{2\pi u \sigma_y \sigma_z} \exp\left(-\frac{y^2}{2\sigma_y^2}\right)\left[\exp\left(-\frac{(z-h)^2}{2\sigma_z^2}\right) + \exp\left(-\frac{(z+h)^2}{2\sigma_z^2}\right)\right]$$

If the source strength q is doubled, then concentration $c(x, y, z)$ is also doubled.

O_3 formation from reaction of VOCs and NO_x

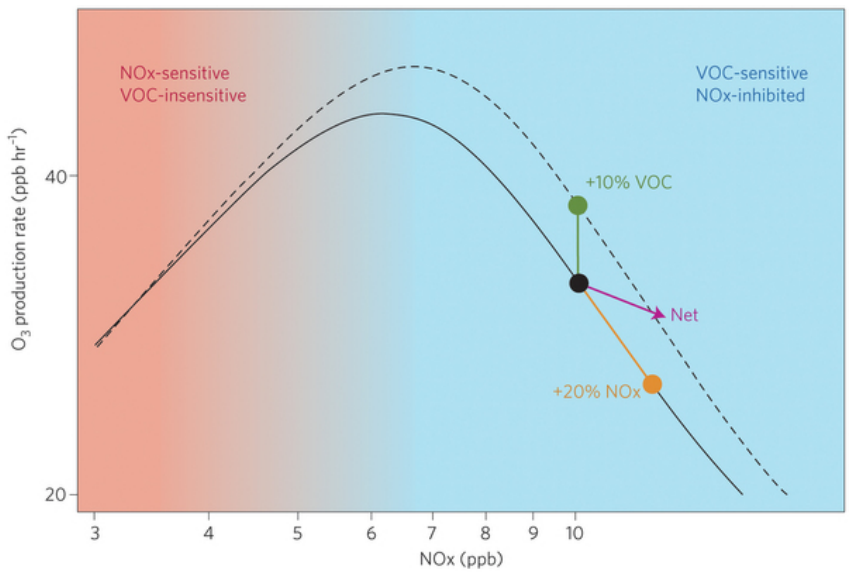

Can we expect homogeneous concentrations within a grid cell?

Grid cells can range from $\sim$4 km to several hundreds of km.

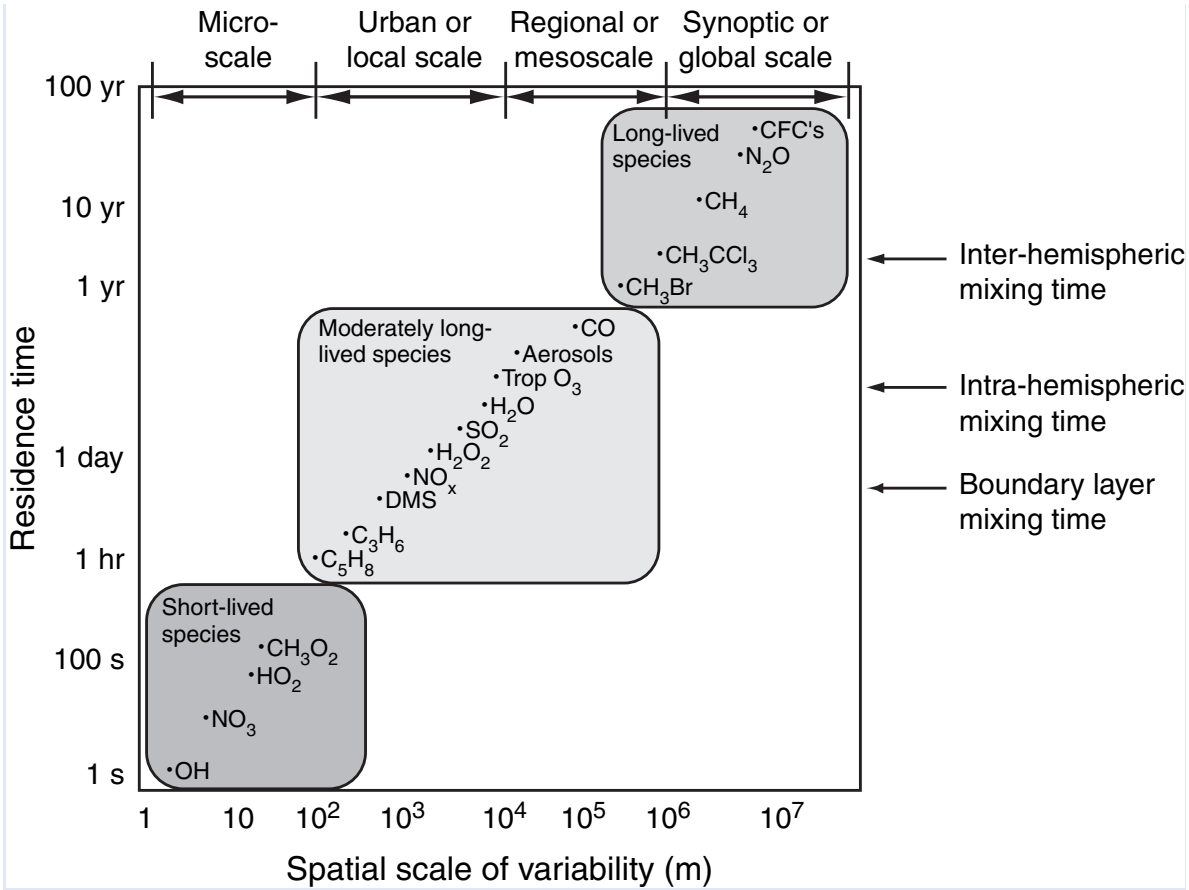

Implications for spatial averaging

Example: ozone formation in Houston.

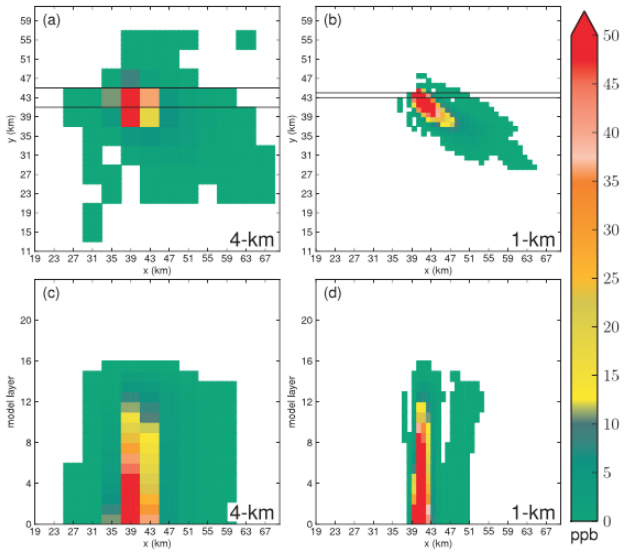

Figure 2. Dispersion of HRVOC release in the (a,c) 4-km and (b,d) 1-km (right) simulation. Vertical dispersion (c,d) is displayed for the row outlined in black in the horizontal dispersion (a,b). The horizontal axis unit is domain kilometers and the vertical axis unit is model layers, which are not displayed proportional to height.

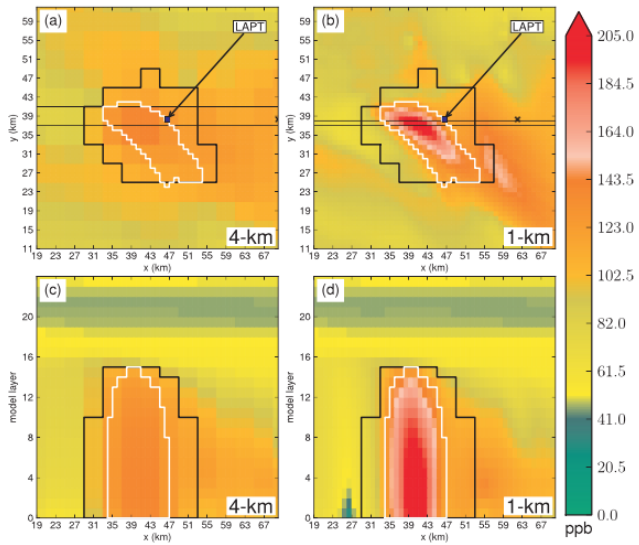

Figure 3. The 4d4r (black outline) and 1d1r (white outline) PAVs overlaid on full chemistry simulated predictions of $[O_3]_{1hr}$ for the peak O_3 hour (4:00 to 5:00 p.m.) in (a,c) the 4-km and (b,d) 1-km resolved simulations. The horizontal view shows the LaPorte monitor (LAPT) location and the location of the $[O_3]_{1hr}$ peak when not using the hypothetical releases (*x*).

Henderson et al., 2012

Note that in addition to dilution, errors can arise if there are sharp concentration gradients within a grid cell (affects mixing of precursors).

Cloud processes

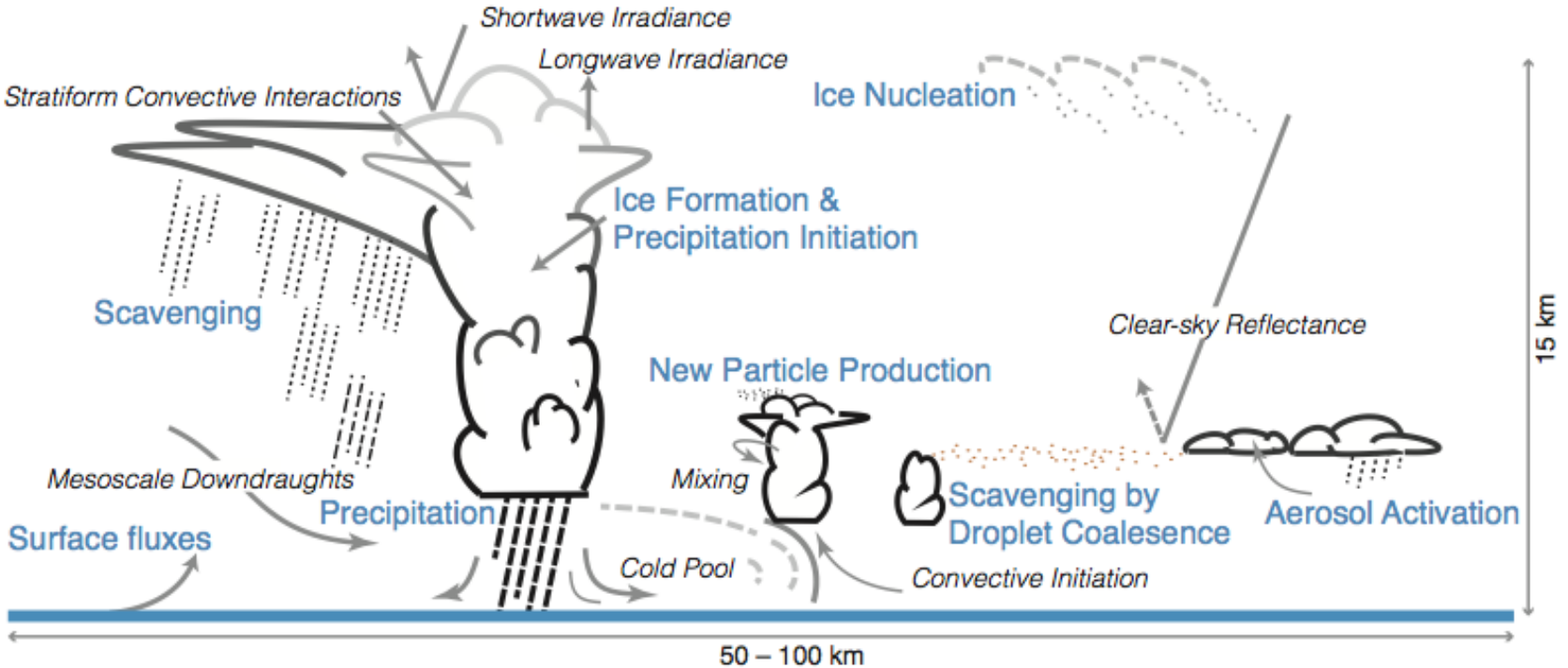

Figure 7.16 | Schematic depicting the myriad aerosol–cloud–precipitation related processes occurring within a typical GCM grid box. The schematic conveys the importance of considering aerosol–cloud–precipitation processes as part of an interactive system encompassing a large range of spatiotemporal scales. Cloud types include low-level stratocumulus and cumulus where research focuses on aerosol activation, mixing between cloudy and environmental air, droplet coalescence and scavenging which results in cloud processing of aerosol particles, and new particle production near clouds; cirrus clouds where a key issue is ice nucleation through homogeneous and heterogeneous freezing; and deep convective clouds where some of the key questions relate to aerosol influences on liquid, ice, and liquid–ice pathways for precipitation formation, cold pool formation and scavenging. These processes influence the shortwave and longwave cloud radiative effect and hence climate. Primary processes that affect aerosol–cloud interactions are labelled in blue while secondary processes that result from and influence aerosol–cloud interactions are in grey.

IPCC, 2013

Parameterizing sub-grid scale processes

Typical length scale for a cloud is a few hundred meters.

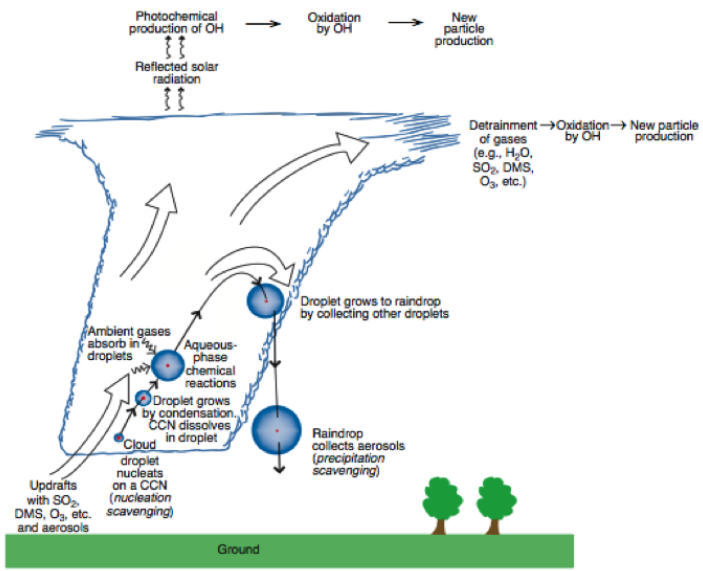

Fig. 6.59 Schematic of cloud and precipitation processes that affect the distribution and nature of chemicals in the atmosphere and the chemical compositions of cloud water and precipitation. The broad arrows indicate airflow. Not drawn to scale.

Wallace and Hobbs, 2006

Typical grid size resolution for GCM is $\sim$100 km.

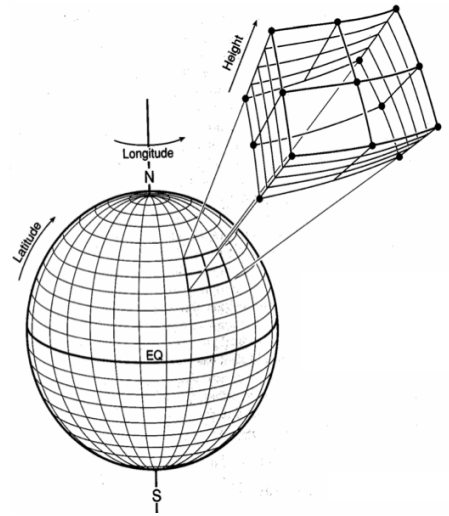

http://seas.harvard.edu

Require cloud parameterizations for:

- Formation
- Precipitation
- Moisture convection
- Radiative properties
- Aqueous-phase processing

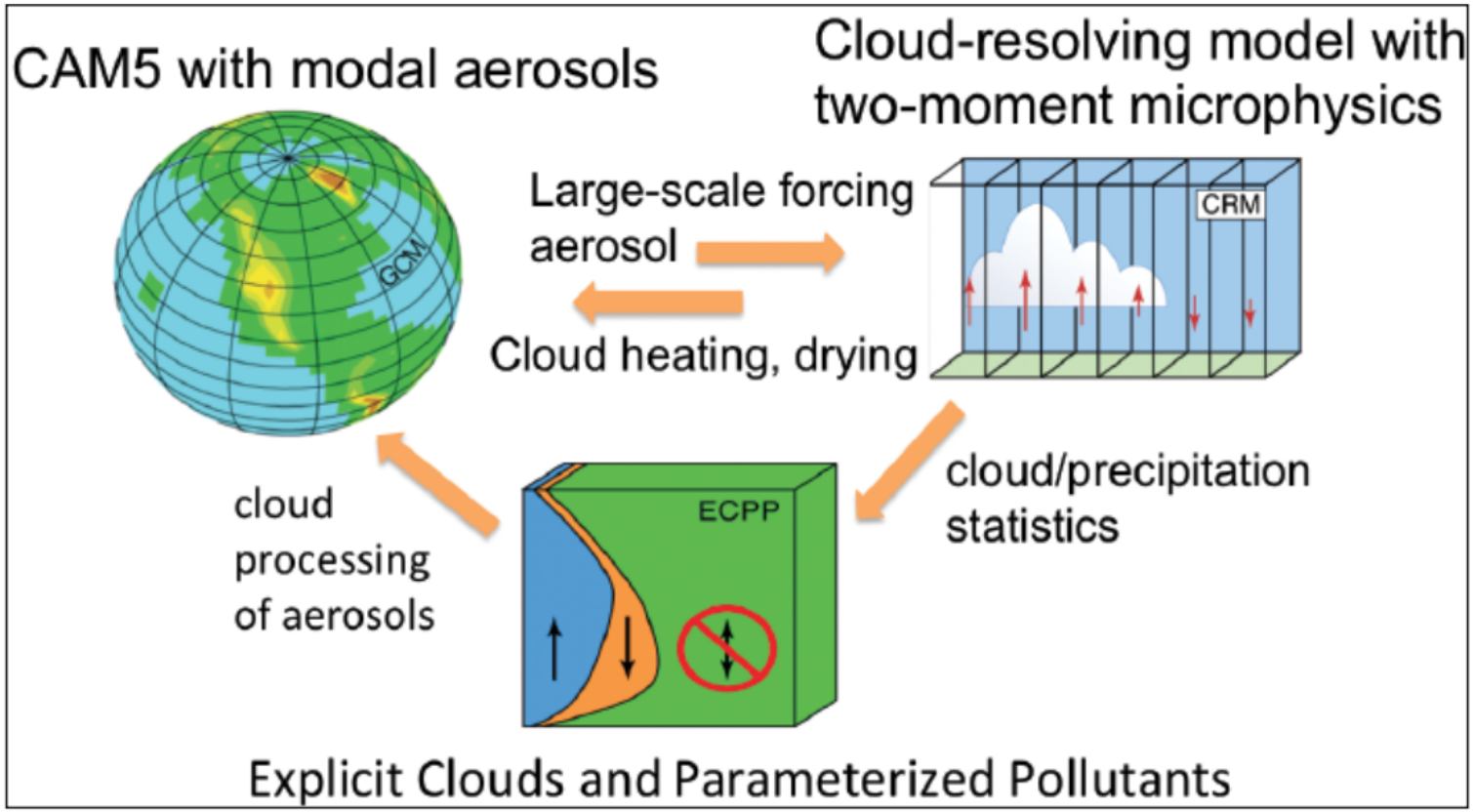

Fig. 1. Configuration of the second generation of the Superparameterized Community Atmosphere Model (SP-CAM). Version 5 of CAM (CAM5, left) simulates the coarse-grid winds and the aerosols used for the radiative heating and two-moment (number and mass) cloud microphysics that drive the cloud-resolving model (CRM). The CRM produces the heating and cloud dynamics that feed back to CAM5 and provides cloud updrafts, cloud liquid water, and precipitation that influence the aerosol through the Explicit Clouds and Parameterized Pollutants (ECPP) module. The ECPP accomplishes this by using cloud information gleaned from the CRM to determine cloud effects on the aerosol. Cloud updrafts are in blue, downdrafts are in orange, and the green area has no vertical motion. Based on Gustafson et al. *[2008, Figure 1].*

Randall, 2013

Bounding predictions

Common approaches to evaluating prediction uncertainty:

- ensemble modeling approach (different chemistry/physics/emission models)
- perturbation of model parameters for a fixed mechanism (also for evaluating sensitivity)

Evaluation with available measurements is critical.

- If our predictions are accurate: are we making making correct predictions for the wrong reasons (by luck)?
- If our predictions are biased: as long as predictions of relative responses to proposed strategies is approximately correct, it is sufficient?

Interpreting prediction errors:

- missing or incorrectly specified emissions?
- missing or incorrectly specified mechanisms/processes?
- resolution problem?

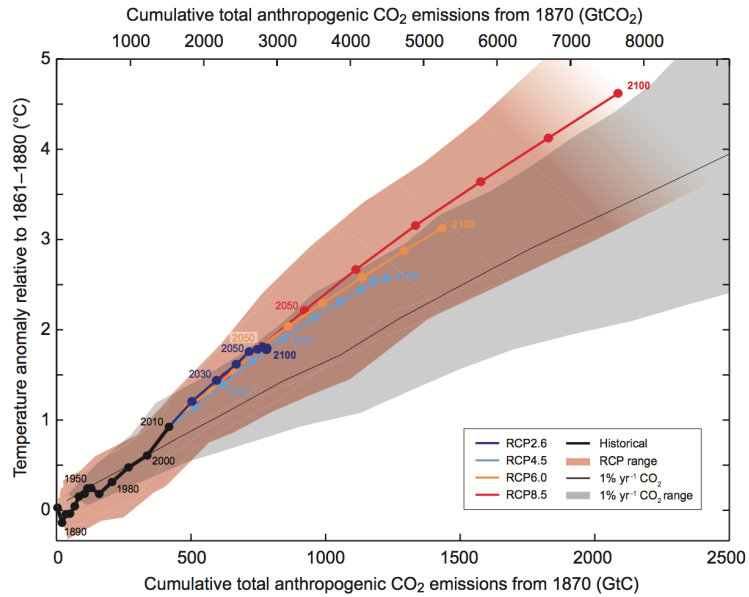

Figure SPM.10 | Global mean surface temperature increase as a function of cumulative total global CO_2 emissions from various lines of evidence. Multi-model results from a hierarchy of climate-carbon cycle models for each RCP until 2100 are shown with coloured lines and decadal means (dots). Some decadal means are labeled for clarity (e.g., 2050 indicating the decade 2040–2049). Model results over the historical period (1860 to 2010) are indicated in black. The coloured plume illustrates the multi-model spread over the four RCP scenarios and fades with the decreasing number of available models in RCP8.5. The multi-model mean and range simulated by CMIP5 models, forced by a CO_2 increase of 1% per year (1% yr^{-1} CO_2 simulations), is given by the thin black line and grey area. For a specific amount of cumulative CO_2 emissions, the 1% per year CO_2 simulations exhibit lower warming than those driven by RCPs, which include additional non-CO_2 forcings. Temperature values are given relative to the 1861–1880 base period, emissions relative to 1870. Decadal averages are connected by straight lines. For further technical details see the Technical Summary Supplementary Material. {Figure 12.45; TS TFE.8, Figure 1}

IPCC, 2013

Atmospheric predictability and chaos

- Predictions of atmospheric motions are highly sensitive to initial conditions: unreliable beyond a few weeks $\Rightarrow$ uncertain weather forecasts (exact state at a future time)
- Climate predictions rely on averaging stochastic fluctuations over time, and try to make statistical statements about a future state.

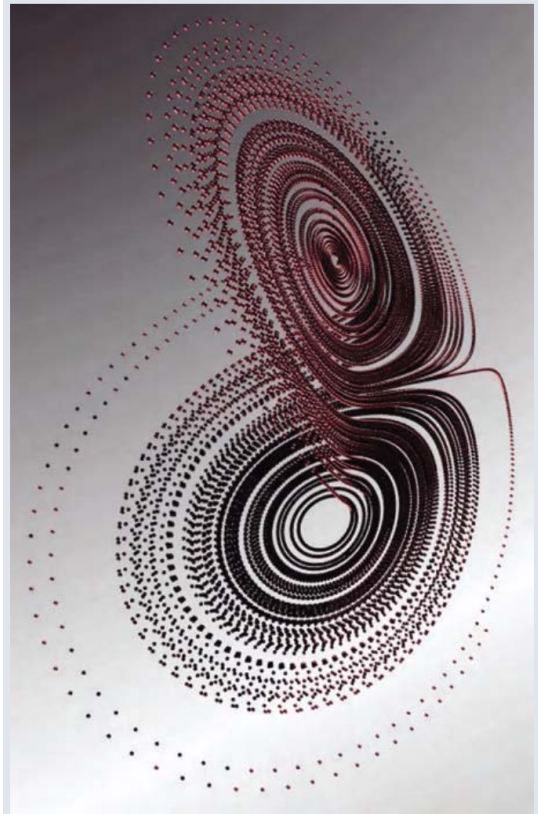

Fig. 1.6 The history of the state of the model used by Lorenz can be represented as a trajectory in a three-dimensional space defined by the amplitudes of the model's three dependent variables. Regime-like behavior is clearly apparent in this rendition. Oscillations around the two different "climate attractors" correspond to the two, distinctly different sets of spirals, which lie in two different planes in the three-dimensional phase space. Transitions between the two regimes occur relatively infrequently. [Permission to use figure from *Nature*, **406**, p. 949 (2000). © Copyright 2000 Nature Publishing Group. Courtesy of Paul Bourke.]

Wallace and Hobbs, 2006

Measurement-model comparison

1. The paired peak prediction accuracy
2. The unpaired peak prediction accuracy
3. The mean normalized bias (MNB) defined by

$$\mathrm{MNB} = \frac{1}{nm}\sum_{i=1}^{n}\sum_{j=1}^{m}\frac{PRED_{i,j} - OBS_{i,j}}{OBS_{i,j}} \qquad (25.133)$$

4. The mean bias (MB) defined by

$$\mathrm{MB} = \frac{1}{nm}\sum_{i=1}^{n}\sum_{j=1}^{m} PRED_{i,j} - OBS_{i,j} \qquad (25.134)$$

5. The mean absolute normalized gross error (MANGE) defined by

$$\mathrm{MANGE} = \frac{1}{nm}\sum_{i=1}^{n}\sum_{j=1}^{m}\frac{|PRED_{i,j} - OBS_{i,j}|}{OBS_{i,j}} \qquad (25.135)$$

6. The mean error (ME) defined by

$$\mathrm{ME} = \frac{1}{nm}\sum_{i=1}^{n}\sum_{j=1}^{m}|PRED_{i,j} - OBS_{i,j}| \qquad (25.136)$$

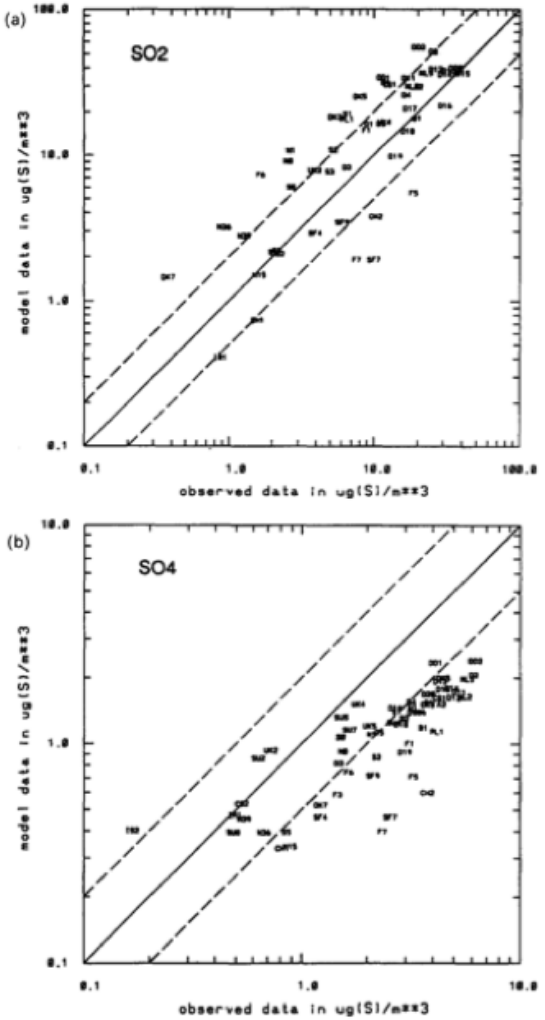

Fig. 5. Observed vs simulated event-averaged near-surface air concentrations for (a) SO_2 and (b) SO_4^{2-} (b) ($\mu g\ Sm^{-3}$). The solid line indicates perfect agreement and the dashed lines indicate agreement within a factor of 0.5 and 2. Station identification is according to EMEP (see also Fig. 1) and 51 and 59 stations were used for the SO_2 and SO_4^{2-} comparison, respectively. The averaging was performed from 20 February to 11 March 1982.

Hass et al., 1993

Modeling the Earth System

General climate models (GCM) vs. earth system models (ESM)

- ESMs include interactions among atmosphere, biosphere, land surface, ocean, and sea ice
- includes additional feedbacks (e.g., changes in vegetation induces reflectivity, moisture exchange)
- must consider tradeoffs among spatial resolution, simulation period, and complexity (number of mechanisms/feedbacks)

Flato, 2011

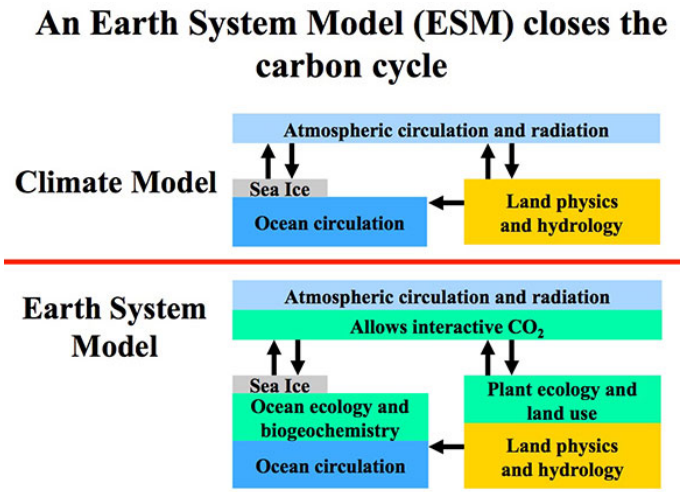

soccom.princeton.edu

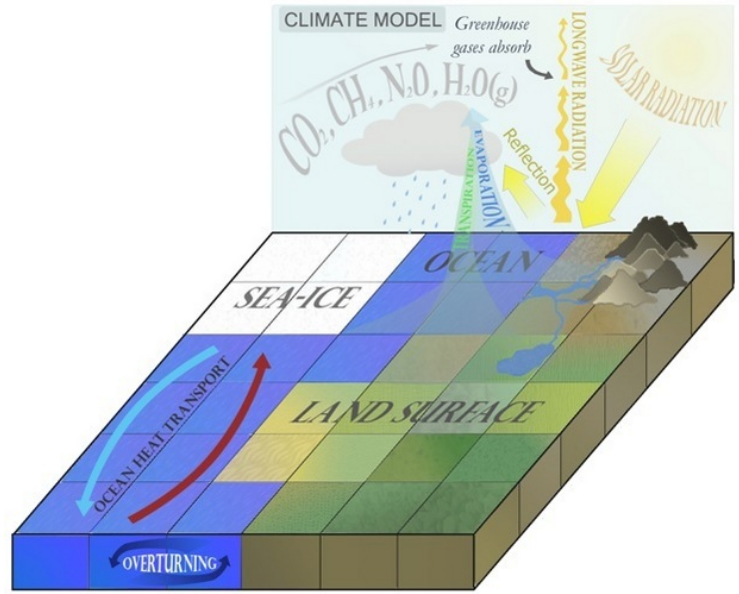

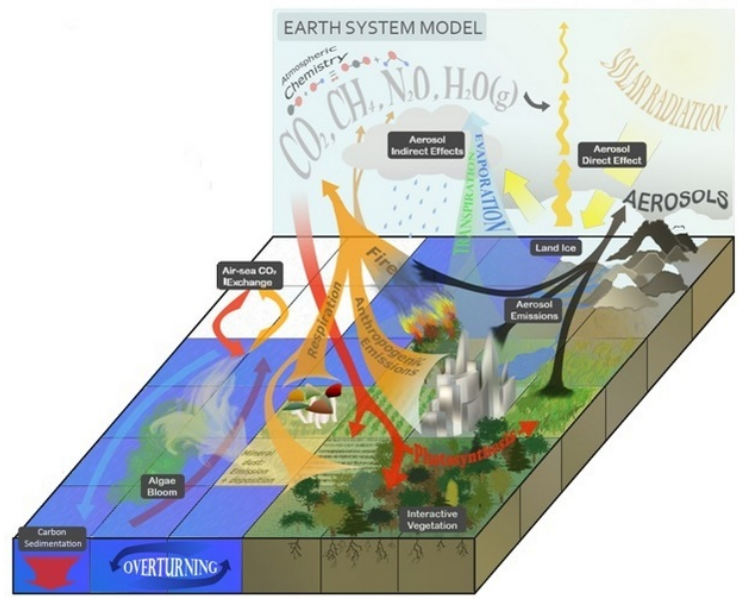

Heavens, N. G., *Nature Education Knowledge*, 2013

Evaluation of climate-relevant variables

- *many variables*: e.g., surface temperature, precipitation, radiative properties, circulation patterns, sea ice extent, carbon flux, heat flux
- *many properties*: e.g., trends, variability, significant changes, extreme events

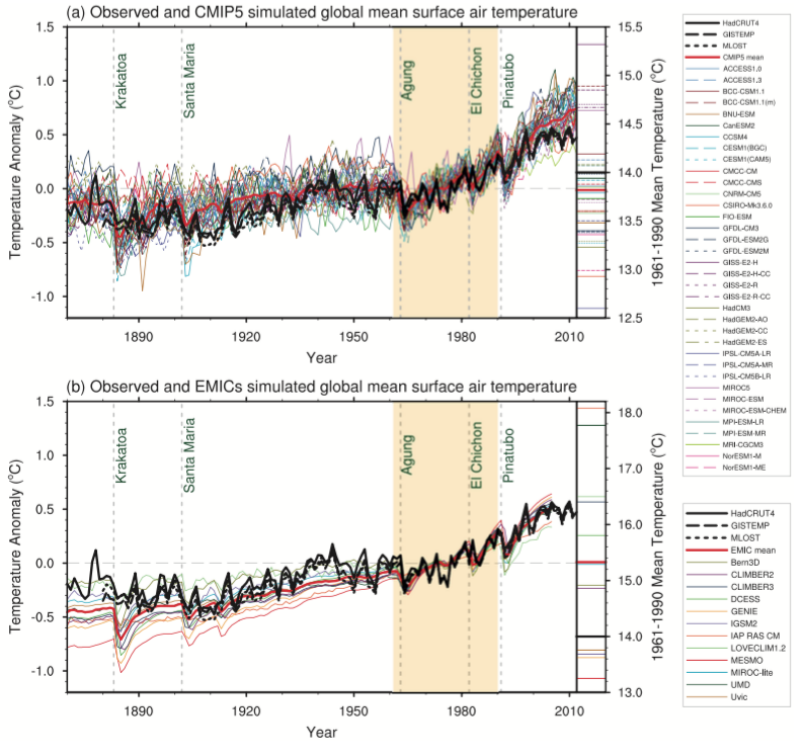

Figure 9.8 | Observed and simulated time series of the anomalies in annual and global mean surface temperature. All anomalies are differences from the 1961–1990 time-mean of each individual time series. The reference period 1961–1990 is indicated by yellow shading; vertical dashed grey lines represent times of major volcanic eruptions. (a) Single simulations for CMIP5 models (thin lines); multi-model mean (thick red line); different observations (thick black lines). Observational data (see Chapter 2) are Hadley Centre/Climatic Research Unit gridded surface temperature data set 4 (HadCRUT4; Morice et al., 2012), Goddard Institute for Space Studies Surface Temperature Analysis (GISTEMP; Hansen et al., 2010) and Merged Land–Ocean Surface Temperature Analysis (MLOST; Vose et al., 2012) and are merged surface temperature (2 m height over land and surface temperature over the ocean). All model results have been sub-sampled using the HadCRUT4 observational data mask (see Chapter 10). Following the CMIP5 protocol (Taylor et al., 2012b), all simulations use specified historical forcings up to and including 2005 and use RCP4.5 after 2005 (see Figure 10.1 and note different reference period used there; results will differ slightly when using alternative RCP scenarios for the post-2005 period). (a) Inset: the global mean surface temperature for the reference period 1961–1990, for each individual model (colours), the CMIP5 multi-model mean (thick red), and the observations (thick black: Jones et al., 1999). (Bottom) Single simulations from available EMIC simulations (thin lines), from Eby et al. (2013). Observational data are the same as in (a). All EMIC simulations ended in 2005 and use the CMIP5 historical forcing scenario. (b) Inset: Same as in (a) but for the EMICs.

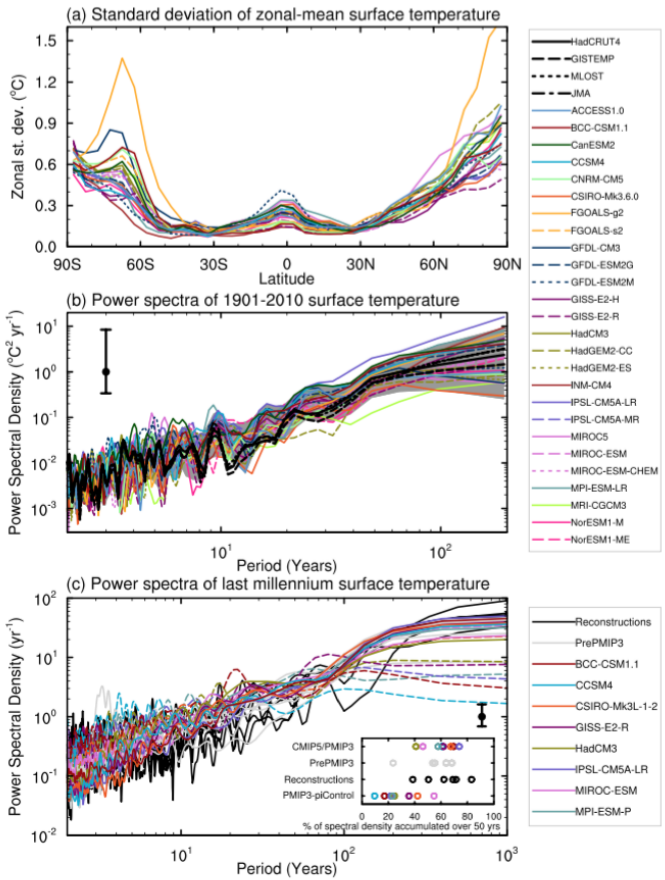

Figure 9.33 | Global climate variability as represented by: (a) Standard deviation of zonal-mean surface temperature of the CMIP5 pre-industrial control simulations (after Jones et al., 2012). (b) Power spectral density for 1901–2010 global mean surface temperature for both historical CMIP5 simulations and the observations (after Jones et al., 2012). The grey shading provides the 5 to 95% range of the simulations. (c) Power spectral density for Northern Hemisphere surface temperature from the CMIP5/ Paleoclimate Modelling Intercomparison Project version 3 (PMIP3) last-millennium simulations (colour, solid) using common external forcing configurations (Schmidt et al., 2012), together with the corresponding pre-industrial simulations (colour, dashed), previous last-millennium AOGCM simulations (black: Fernandez-Donado et al., 2013), and temperature reconstructions from different proxy records (see Section 5.3.5). For comparison between model results and proxy records, the spectra in (c) have been computed from normalized Northern Hemisphere time series. The small panel included in the bottom panel shows for the different models and reconstructions the percentage of spectral density cumulated for periods longer than 50 years, to highlight the differences between unforced (pre-industrial control) and forced (PMIP3 and pre-PMIP3) simulations, compared to temperature reconstruction for the longer time scales. In (b) and (c) the spectra have been computed using a Tukey–Hanning filter of width 97 and 100 years, respectively. The model outputs were not detrended, except for the MIROC-ESM millennium simulation. The 5 to 95% intervals (vertical lines) provide the accuracy of the power spectra estimated given a typical length of 110 years for (b) and 1150 years for (c).

CMIP5: Coupled Model Intercomparison Project Phase 5

EMICs: Earth system Models of Intermediate Complexity

IPCC, 2013

“The Greenhouse Gamble”

How much would you pay to switch wheels?

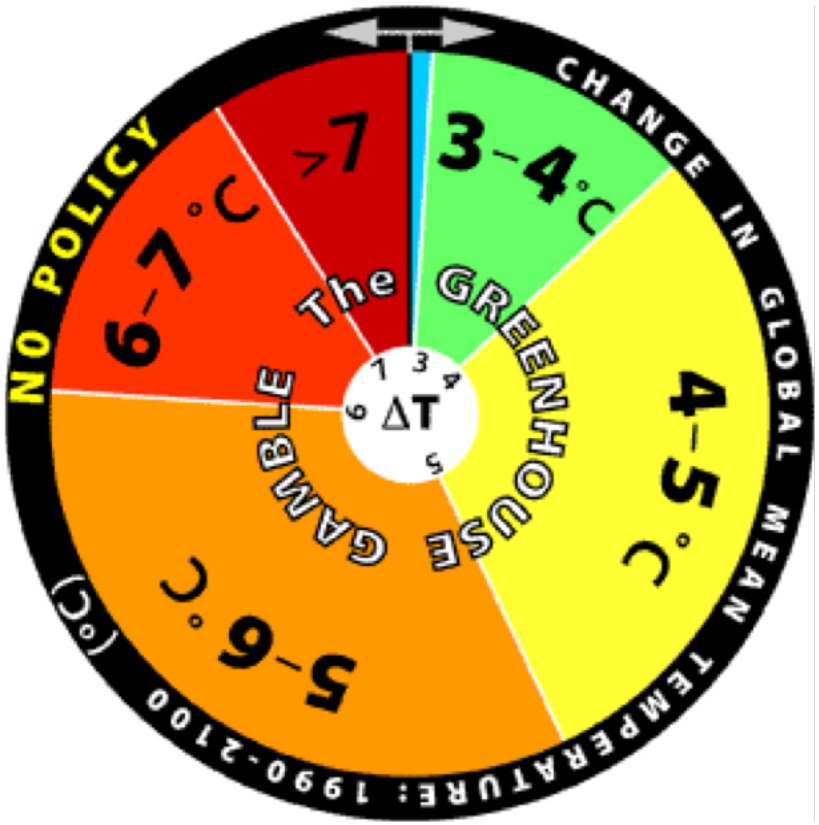

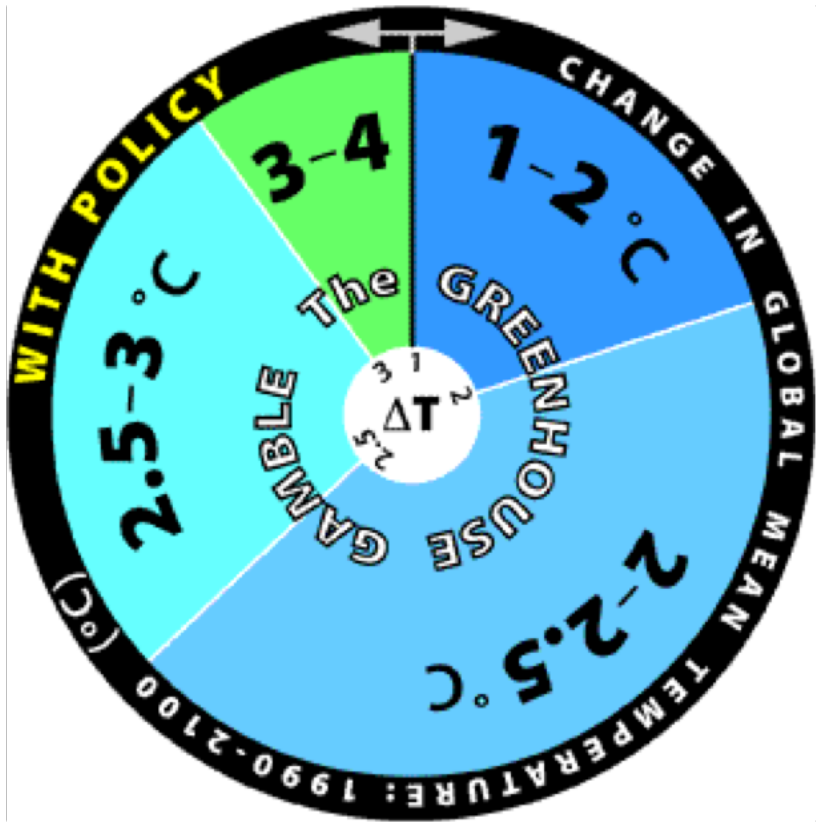

MIT Global Change

Model for instantaneous mixing

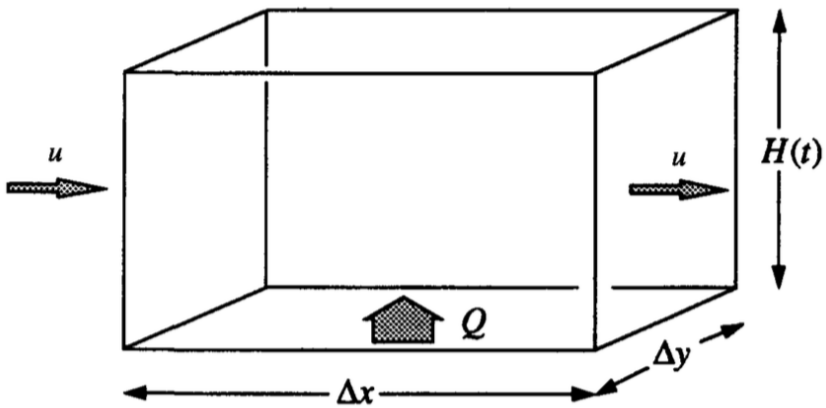

FIGURE 25.4 Box model framework.

Seinfeld and Pandis (2006)

Considering mixing layer height $H(t)$, the Lagrangian (and Eulerian) formulation for a box model is

$$\frac{dc_i}{dt} = \frac{q_i}{H(t)} \quad \text{emission}$$

$$+ R_i \quad \text{reaction}$$

$$- \frac{v_{d,i}}{H(t)} c_i \quad \text{dry deposition}$$

$$+ \frac{c_i^a - c_i}{H(t)} \frac{dH}{dt} \mathcal{U}\left(\frac{dH}{dt}\right) \quad \text{entrainment}$$

$$\left(+ \frac{c_i^0 - c_i}{\tau_r}\right) \quad \text{advection}$$

where $c_i^0 = c_i(t=0)$, $c_i^a = c_i^a(t)$, $\mathcal{U} =$ Heaviside unit step function.

Modeling plume dispersion

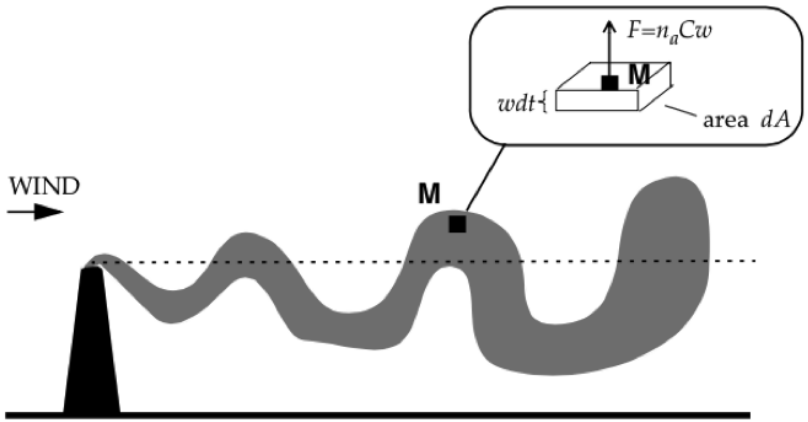

Figure 4-20 Instantaneous smokestack plume

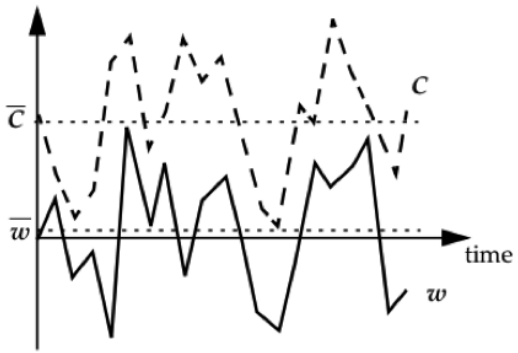

Figure 4-21 Time series of C and w measured at a fixed point M. $\overline{C}$ and $\overline{w}$ are the time-averaged values.

Jacob (1999)

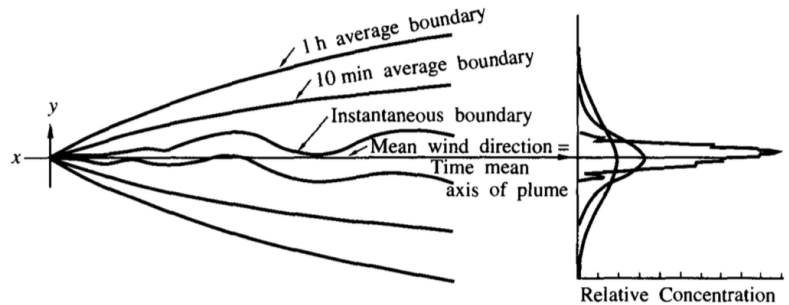

FIGURE 18.2 Plume boundaries and concentration distributions of a plume at different averaging times.

Seinfeld and Pandis (2006)

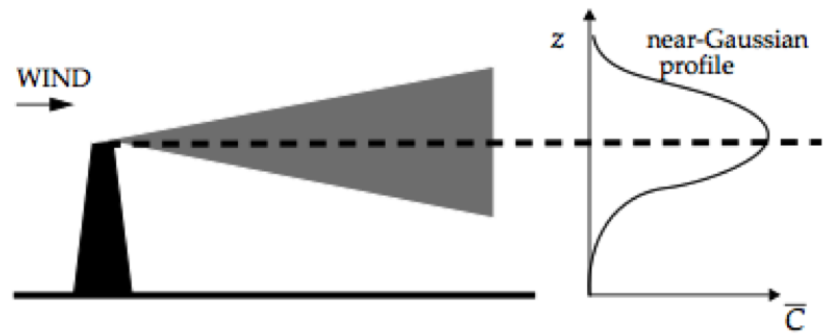

Figure 4-23 Time-averaged smokestack plume

Jacob (1999)

Gaussian plume model from advection-diffusion equations

Let $c = \overline{c}$ and $u = \overline{u}$. Consider dispersion equation for $\mathbf{u} = (u_x, 0, 0)$, $q = q(0, 0, h, 0)$, total reflection at $z = 0$, extending over the domain $0 \leq z \leq \infty$. $\delta(\cdot)$ is the Dirac delta function. S is the source strength in mass concentration per unit time; q is the source strength in mass per unit time.

Instantaneous release:

$$\frac{\partial c}{\partial t} + u_x \frac{\partial c}{\partial x} = K_{xx} \frac{\partial^2 c}{\partial x^2} + K_{yy} \frac{\partial^2 c}{\partial y^2} + K_{zz} \frac{\partial^2 c}{\partial z^2}$$

$$\begin{aligned} c(x, y, z, 0) &= S\delta(t) \\ c(x, y, z, t) &= 0 \qquad x, y, z \to \pm\infty \\ K_{zz} \frac{\partial c}{\partial z} &= 0 \qquad z = 0 \\ q &= S\delta(x)\delta(y)\delta(z - h) \end{aligned}$$

Continuous source:

$$\begin{aligned} \frac{\partial c}{\partial t} + u_x \frac{\partial c}{\partial x} =& K_{xx} \frac{\partial^2 c}{\partial x^2} + K_{yy} \frac{\partial^2 c}{\partial y^2} + K_{zz} \frac{\partial^2 c}{\partial z^2} \\ &+ S(x, y, z, t) \end{aligned}$$

$$\begin{aligned} c(x, y, z, 0) &= 0 \\ c(x, y, z, t) &= 0 \qquad x, y, z \to \pm\infty \\ K_{zz} \frac{\partial c}{\partial z} &= 0 \qquad z = 0 \\ q &= S\delta(x)\delta(y)\delta(z - h) \\ &= \int\int u_x c(x, y, z, t) dydz \end{aligned}$$

Assume constant diffusivities. Let

$$\sigma_x^2 = 2K_{xx}t, \quad \sigma_y^2 = 2K_{yy}t, \quad \text{and} \quad \sigma_z^2 = 2K_{zz}t$$

Gaussian plume model

Total reflection at surface

Gaussian puff model (solution to instantaneous release):

$$c(x,y,z,t) = \frac{q}{(2\pi)^{3/2}\sigma_x\sigma_y\sigma_z}\exp\left(-\frac{(x-ut)^2}{2\sigma_x^2}-\frac{y^2}{2\sigma_y^2}\right) \times\left[\exp\left(-\frac{(z-h)^2}{2\sigma_z^2}\right)+\exp\left(-\frac{(z+h)^2}{2\sigma_z^2}\right)\right]$$

Gaussian plume model (solution to continuous release):

$$c(x,y,z) = \frac{q}{2\pi u\sigma_y\sigma_z}\exp\left(-\frac{y^2}{2\sigma_y^2}\right)\left[\exp\left(-\frac{(z-h)^2}{2\sigma_z^2}\right)+\exp\left(-\frac{(z+h)^2}{2\sigma_z^2}\right)\right]$$

We often use a reference height of $h = h_s + \Delta h$ to account for plume rise (Δh) on top of the stack (h_s).

Conceptualizing total reflection

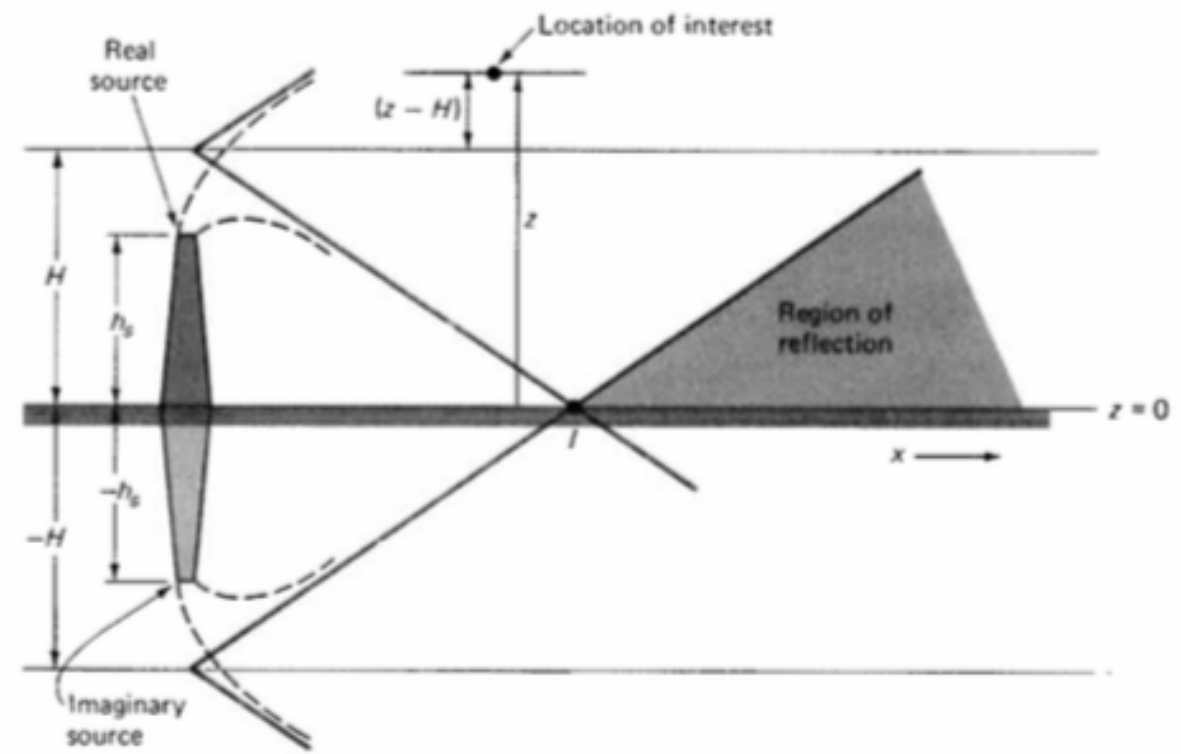

FIGURE 4-3 Use of an imaginary source to describe mathematically gaseous reflection at the surface of the earth.

Wark et al. (1998)

Estimating dispersion parameters for continuous release

Dispersion parameters σ_y and σ_z can be estimated from theoretical considerations, but may require environmental variables which are not readily available. Widely used parameterizations are based on atmospheric stability classes. Commonly used parameterizations were developed with 10 minute sampling times, but are often assumed to represent one-hour averages.

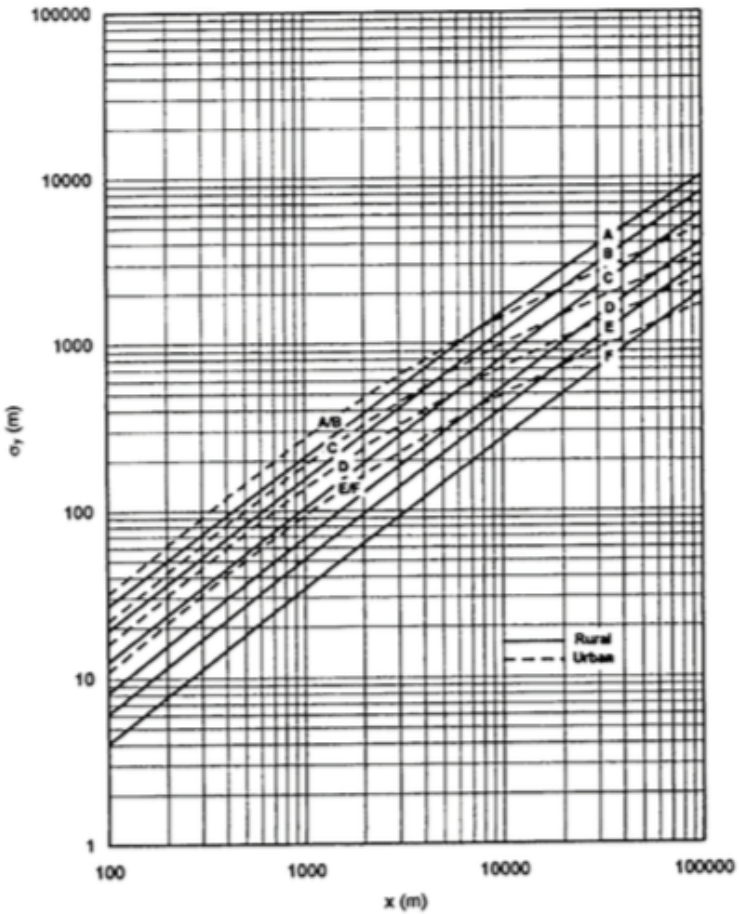

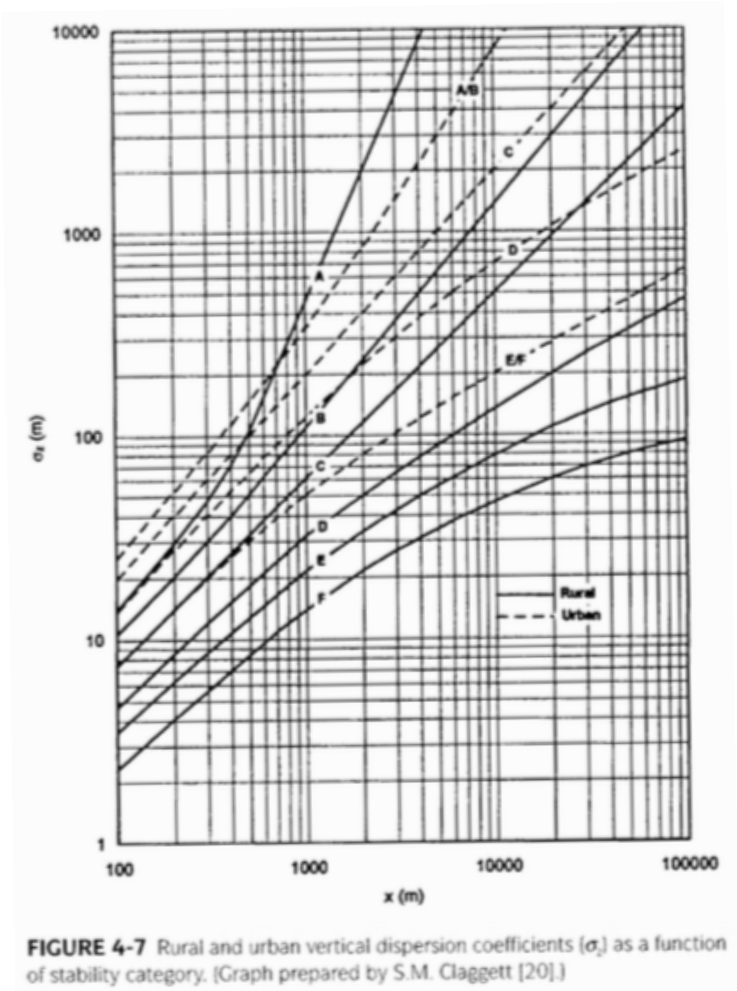

FIGURE 4-7 Rural and urban vertical dispersion coefficients (σ_z) as a function of stability category. (Graph prepared by S.M. Claggett [20].)

Rural parameterization

Parameterization for rural values ("Pasquil-Gifford" curves) for downwind distance x (solid lines in Figures 4-6 and 4-7):

$$\sigma_y = 465.11628 \cdot x \cdot \tan(TH)$$

$$TH = 0.01745[c - d\ln(x)]$$

$$\sigma_z = a \cdot x^b$$

Note that x is in km and σs are in m.

TABLE 4-1 Parameters Used to Calculate Pasquill-Gifford σ_y

Pasquill Stability Category	*c*	*d*
A	24.1670	2.5334
B	18.3330	1.8096
C	12.5000	1.0857
D	8.3330	0.72382
E	6.2500	0.54287
F	4.1667	0.36191

TABLE 4-2 Parameters Used to Calculate Pasquill-Gifford σ_z

Pasquill Stability Category	x (km)	a	b
A*	<.10	122.800	0.94470
	0.10 – 0.15	158.080	1.05420
	0.16 – 0.20	170.220	1.09320
	0.21 – 0.25	179.520	1.12620
	0.26 – 0.30	217.410	1.26440
	0.31 – 0.40	258.890	1.40940
	0.41 – 0.50	346.750	1.72830
	0.51 – 3.11	453.850	2.11660
	>3.11	**	**
B*	<.20	90.673	0.93198
	0.21 – 0.40	98.483	0.98332
	>0.40	109.300	1.09710
C*	All	61.141	0.91465
D	<.30	34.459	0.86974
	0.31 – 1.00	32.093	0.81066
	1.01 – 3.00	32.093	0.64403
	3.01 – 10.00	33.504	0.60486
	10.01 – 30.00	36.650	0.56589
	>30.00	44.053	0.51179
E	<.10	24.260	0.83660
	.010 – 0.30	23.331	0.81956
	0.31 – 1.00	21.628	0.75660
	1.01 – 2.00	21.628	0.63077
	2.01 – 4.00	22.534	0.57154
	4.01 – 10.00	24.703	0.50527
	10.01 – 20.00	26.970	0.46713
	20.01 – 40.00	35.420	0.37615
	>40.00	47.618	0.29592
F	<.20	15.209	0.81558
	0.21 – 0.70	14.457	0.78407
	0.71 – 1.00	13.953	0.68465
	1.01 – 2.00	13.953	0.63227
	2.01 – 3.00	14.823	0.54503
	3.01 – 7.00	16.187	0.46490
	7.01 – 15.00	17.836	0.41507
	15.01 – 30.00	22.651	0.32681
	30.01 – 60.00	27.074	0.27436
	>60.00	34.219	0.21716

*If the calculated value of σ_z exceeds 5000 m, σ_z is set to 5000 m.
** σ_z is equal to 5000 m.

Wark et al. (1998)

Urban parameterization

Parameterization for urban values ("McElroy-Pooler" curves) for downwind distance x (dashed lines in Figures 4-6 and 4-7):

TABLE 4-3 Briggs Formulas Used to Calculate McElroy-Pooler σ_y

Pasquill Stability Category	σ_y (meters)*
A	$0.32\,x\,(1.0 + 0.0004\,x)^{-1/2}$
B	$0.32\,x\,(1.0 + 0.0004\,x)^{-1/2}$
C	$0.22\,x\,(1.0 + 0.0004\,x)^{-1/2}$
D	$0.16\,x\,(1.0 + 0.0004\,x)^{-1/2}$
E	$0.11\,x\,(1.0 + 0.0004\,x)^{-1/2}$
F	$0.11\,x\,(1.0 + 0.0004\,x)^{-1/2}$

*Where x is in meters

TABLE 4-4 Briggs Formulas Used to Calculate McElroy-Pooler σ_z

Pasquill Stability Category	σ_z (meters)*
A	$0.24\,x\,(1.0 + 0.001\,x)^{1/2}$
B	$0.24\,x\,(1.0 + 0.001\,x)^{1/2}$
C	$0.20\,x$
D	$0.14\,x\,(1.0 + 0.003\,x)^{-1/2}$
E	$0.08\,x\,(1.0 + 0.015\,x)^{-1/2}$
F	$0.08\,x\,(1.0 + 0.015\,x)^{-1/2}$

*Where x is in meters.

Wark et al. (1998)

Stability classification

TABLE 3-1 Key to Stability Classes[a]

Surface Wind Speed at 10 m (m/s)	*Day*			*Night*	
	Incoming Solar Radiation			*Cloud Cover*	
	Strong	Moderate	Slight	Thinly Overcast or ≥50% Clouds	Mostly Clear or $\leq \frac{3}{8}$ Clouds
<2	A	A–B	B	—	—
2–3	A–B	B	C	E	F
3–5	B	B–C	C	D	E
5–6	C	C–D	D	D	D
>6	C	D	D	D	D

[a]The neutral class, D, should be assumed for overcast conditions during day or night.
Source: D. B. Turner, *Workbook of Atmospheric Dispersion Estimates*, Washington, D.C.: HEW, 1969.

TABLE 3-2 Comparison of Different Stability Techniques

Pasquill	dT/dz[a] (° C/100m)	σ_θ[a]	σ_φ
A	≤ −1.9	≥ 22.5°	≥12°
B	> −1.9 but ≤ −1.7	≥ 17.5 but < 22.5	≥10 but < 12
C	> −1.7 but ≤ −1.5	≥ 12.5 but < 17.5	≥ 7.8 but < 10
D	> −1.5 but ≤ −0.5	≥ 7.5 but < 12.5	≥ 5.0 but < 7.8
E	> −0.5 but ≤ 1.5	≥ 3.8 but < 7.5	≥ 2.4 but < 5.0
F	> 1.5 but ≤ 4.0	≥ 2.1 but < 3.8	< 2.4
G	> 4.0	< 2.1	—

[a]Proposed revision to Regulatory Guide 1.23. Nuclear Regulatory Commission, Sept. 1980.

Wark et al. (1998)

Dispersion parameters for instantaneous release

Instantaneous release model requires use of dispersion parameters that are representative over shorter averaging times. Typically, $\sigma_x \approx \sigma_y$ is assumed.

TABLE 4.7 Instantaneous Values for σ_y and σ_z in meters [11]

Parameter	Stability Condition	Equation*
σ_y	Unstable	$\sigma_y = 0.14\,(x)^{0.92}$
	Neutral	$\sigma_y = 0.06\,(x)^{0.92}$
	Very Stable	$\sigma_y = 0.02\,(x)^{0.89}$
σ_z	Unstable	$\sigma_z = 0.53\,(x)^{0.73}$
	Neutral	$\sigma_z = 0.15\,(x)^{0.70}$
	Very Stable	$\sigma_z = 0.05\,(x)^{0.61}$

*x is the distance downwind in meters.

Wark et al. (1998)

Further reading

Jacob, D. *Introduction to Atmospheric Chemistry*. Princeton University Press, 1999.

Jacobson, M. Z. *Fundamentals of Atmospheric Modeling*. 2nd ed. Cambridge University Press, 2005.

Seinfeld, J. H. & Pandis, S. N. *Atmospheric Chemistry and Physics: From Air Pollution to Climate Change*. John Wiley & Sons, 2006.

Sportisse, B. *Fundamentals in Air Pollution: From Processes to Modelling*. Springer, 2010.

Wallace, J. M., and Hobbs, P. V. *Atmospheric Science: An Introductory Survey*. Academic Press, 2006.